I. 8. Evaluation of Ductile-brittle Transition Behavior of Helium-Implanted Reduced Activation Martensitic Steel F82H by Miniature Charpy Specimens

Hasegawa A., Wakabayashi E., Tanaka K., Abe K., and Jitsukawa S.[*]

Department of Quantum Science and Energy Engineering, Tohoku University
Japan Atomic Energy Research Institute, Tokai Lab., Shirakata-shirane, Tokai, Japan[*]

Introduction

Helium induced embrittlement is one of the critical issues of fusion structural materials in which several thousands at.ppm of helium is estimated to be generated during reactor operation. It is well known that a small amount of helium enhances irradiation embrittlement of austenitic steels[1-3] and some vanadium alloys[4,5] in the tests at relatively high temperatures accompanied by the change in the fracture mode from transgranular to intergarnular cracking. Microstructural observations revealed that many bubbles, which were considered to be helium bubbles, existed at grain boundaries, indicating that the helium atoms in the matrix of these materials diffused to form bubbles at grain boundaries during irradiation and/or testing at a high temperature. In contrast, it was reported that the martensitic steels were highly resistant to helium bubble-induced grain boundary embrittlement[6-8] at high temperatures. High resistance to the bubble formation in the martensitic steels is considered to be attributed to trapping of helium atoms and point defects in the martensitic structure or dislocations, lath boundaries and carbides in high density which prevent helium atoms segregating to form helium bubbles at grain boundaries.

Ductile-brittle transition behavior is characteristic to martensitic steels, and irradiation hardening usually results in an increase in the transition temperature. It is expected that the trapped helium atoms in the martensitic structure would enhance irradiation hardening of the matrix and resultantly transgranular embrittlement at low temperatures. As for the effects of helium on the ductile-brittle transition behavior of the martensitic steels, there have been done several studies relating to the effects of so called

transmutation helium. Isotope tailoring experiments on helium effects utilizing nuclear transmutation helium from nickel[9-12] and boron[13] showed that the increase in the composition of nickel or boron caused severer irradiation embrittlement in the martensitic steels, and the enhanced embrittlement, which was usually accompanied by severer irradiation hardening, was attributed to the helium transmuted from nickel or boron. It is, however, not made clear that the transmutation helium in itself really induces low temperature embrittlement, since the addition of boron or nickel results in the change in the martensitic structure or properties of the steel[14].

Helium implantation technique is more effective to evaluate helium effects directly and many investigations have been performed for the martensitic steels. Since the range of the implantation is usually smaller than 0.2 mm, the experiments have been often limited to microstructural observation, hardness measurement and tensile test with thin specimens. We had already reported the He effect of DBTT of martensitic steels JLF-1 using 650 appm He implanted TEM disks by means of small punch test[15]. Increase of DBTT caused by irradiation hardening was observed, however, grainboundary embrittlement was not observed. It is well known that charpy impact test is more appropriate to estimate DBTT behavior, but relatively larger specimen volume is needed for charpy impact test. Small specimen test technique have been developed to evaluate mechanical properties of irradiated specimen. Miniature charpy test method is one of example of the small specimen test technique. Specimen size is almost 1/10 of the standard specimen such as ASTM standard or JIS standard. This methods have already been applied to neutron irradiation studies but not been applied to high energy ion-beam irradiation experiments.

In this study, to study the DBTT behavior of reduced activation martensitic steels by means of charpy impact test method, we improved irradiation apparatus of materials irradiation course of CYRIC, and evaluate the effects the DBTT behavior.

Experimental

Figure 1 shows a overview of 42-beam course for material irradiation in target room 4. Irradiation chamber was installed at the end of this beam line. The chamber is evacuated up to 1 x 10^{-6} Torr by a turbo pump. Various type of material irradiation experiments are available. Figure 2 shows a specimen loading system which has four different stage positions. Two specimen holders are installed in this picture. Upper position is for room temperature irradiation, lower position is for high temperature irradiation up to 600°C. Water cooling system is installed at upper two positions and

heating system using a sheath heater are available at all positions. Specimen temperature is monitored using thermocouples and an infrared pyrometer. A tandem type energy degrader system are also installed in this irradiation chamber. This system consists two rotating wheels. The first wheel consists of 5 different thickness of aluminum foils, and the second wheel consists of 105 different thickness of aluminum foils. Therefore total 525 different thickness aluminum foils across the incident beam line. Figure 3 shows drawings of a rotating wheel, and Fig. 4 shows a schematic illustration of a tandem type energy degrader system. Using this energy degrader system, irradiated ions can be implanted almost homogeneously from the irradiated surface to its projected range.

In order to evaluate DBTT behavior, a small charpy specimen were used. The size and shape, and its notch configuration are shown in Fig. 5 and Fig. 6, respectively. F82H, a 8Cr-2W base martensitic steels, was used as sample. It is reference material of RAM in IEA research activities for fusion rector materials. An ingot of IEA heat F82H heat-treated by standard procedures were supplied from JAERI. Charpy specimens were fabricated from this ingot. Nine charpy specimens were loaded in a specimen holder at once. Thermocouples were welded on the specimen.

Alpha particles beam accelerated to 50 MeV was used for He implantation. The projected range of this ion beam in Iron was about 380 μm. Implanted He concentration of the specimen was about 50 appm and the displacement damage was about 0.04 dpa after 10 h irradiation. In order to obtain higher implanted He concentration during a limited irradiation time, the ion beam was scanned horizontally only the periphery of center V notch area of the specimens. Irradiation temperature of the irradiated specimen area were below 90°C in the room temperature irradiation, and 500°C in the high temperature irradiation. The specimen temperature control system, temperature monitoring system, specimen loading system and energy degrader system were controlled by a computer through internet using PLC system.

After the irradiation, these specimens were moved to RI laboratory of Faculty of Engineering of Tohoku University to measure hardness using a Vickers hardness tester, and then these were shipped to hot laboratory of Oarai branch of IMR, Tohoku University to carry out impact test. The instrumented charpy impact test were conducted in a hot cell of Oarai laboratory at temperature between -140°C and -100°C. After the charpy impact test, these specimens were shipped to Alpha-emitter laboratory of IMR (Sendai), and fracture surface observation was conducted using a scanning electron microscope.

Results

Figure 7 shows result of hardness before and after irradiation. Hardness increased after room temperature irradiation. The hardness of implanted specimen almost recovered after heat treatment at 550℃ for 1hour. The hardening was also observed clearly in the specimen which were irradiated at 500℃.

Typical examples of load / displacement curves obtained by the charpy impact test at various test temperature is shown in Fig. 8-(a). The area below each load/displacement curve corresponds to the absorbed energy to rupture at each test temperature. Figure 8-(b) summarizes test temperature dependence of absorbed energy of unimplanted specimen. Fracture mode transient from ductile mode to brittle mode are clearly observed in this figure. In Fig. 8-(b) ductile brittle transient temperature(DBTT) is about -125°C. Below -140°C, specimen ruptured brittle. The typical fracture surface of the specimen is shown in Fig. 9. The rupture mode was cleavage. The temperature above -100°C, specimen ruptured ductile. The dimple pattern was observed on fracture surface. Figure 11 shows the typical ductile fracture pattern of specimen. Between -140°C and -100°C is transient temperature region. Specimen tested and ruptured at this temperature region shows mix fracture mode. Figure 10 shows typical fracture surface tested at the transient temperature

Figure 12 is a summary of DBTT curves of He implanted/unimplanted specimens. DBTT increased about 10°C after the He implantation at 30°C. In the case of higher temperature irradiation, temperature range of transient mode increased but brittle mode area still remains at lower temperature. The detail analysis using fracture analysis is in progress. Considering about the temperature shift and data dispersion, implantation up to higher concentration of He (more than 1000 appm) is needed to clarify the He effects on fracture mode change of reduced activation martensitic steels.

Summary

(1) Material irradiation chamber was moved and improved for higher temperature irradiation. Energy degrader system and multi-stage specimen loading stage with cooling and heating system controlled by PC were installed. This system can be applied for higher energy and higher current beam irradiation.

(2) Helium implantation to 50 appm at RT and 500°C were conducted. Irradiation hardening was detected and DBTT shift by He implantation was observed. The effect of He on fracture mode change was not observed.

Acknowledgements

The authors are grateful to the staffs in the CYRIC of Tohoku University relating to beam transport and irradiation experiments. The authors are also grateful to Mr. T. Takahashi, Mr. K. Komatsu and Mr.T. Nagaya of machine shop of Dept. of Quantum Science and Energy Engineering, Tohoku University for fabrication of specimen loading system and energy degrader.

References

1) Schroeder H. and Batfalsky P., J. Nucl. Mater. **117** (1983) 287.
2) Trinkaus H., J. Nucl. Mater. **133&134** (1985) 105.
3) Schroeder H., J. Nucl. Mater. **155-157** (1988) 1032.
4) Braski D.N. and Ramey D.W., Effects Radiation on Materials, ASTM STP **870** (1985) 1211.
5) Satou M., Koide H., Hasegawa A., Abe K., Kayano H. and Matsui H., J. Nucl. Mater. **233-237** (1996) 447.
6) Stamm U. and Schroeder H., J. Nucl. Mater. **155-157** (1988) 1059.
7) Moslang A. and Preininger D., J. Nucl. Mater. **155-157** (1988) 1064.
8) Moslang A. and Preininger D., J. Nucl. Mater. **191-194** (1992) 910.
9) Klueh R.L. and Vitek J.M., J. Nucl. Mater. **150** (1987) 272.
10) Klueh R.L. and Vitek J.M., J. Nucl. Mater. **161** (1989) 13.
11) Klueh R.L. and Alexander D.J., J. Nucl. Mater. **179-181** (1991)733.
12) Klueh R.L. and Maziasz P.J., J. Nucl. Mater. **187** (1992) 43.
13) Lindau R., Moslang A., Preininger D., Rieth M. and Rohrig H.D., J. Nucl. Mater. **271-272** (1999) 450.
14) Heinisch H. L., J. Nucl. Mater. **155-157** (1988) 121.
15) Kimura A., Morimura T., Kasada R., Matsui H., Hasegawa A. and Abe K., *Effects of Radiation on Materials, 19th International Symposium, ASTM STP 1366*, M.L. Hamilton, A.S. Kumar, S.T. Rosinski and M.L. Grossbeck, Eds., American Society for Testing and Materials, 1999.

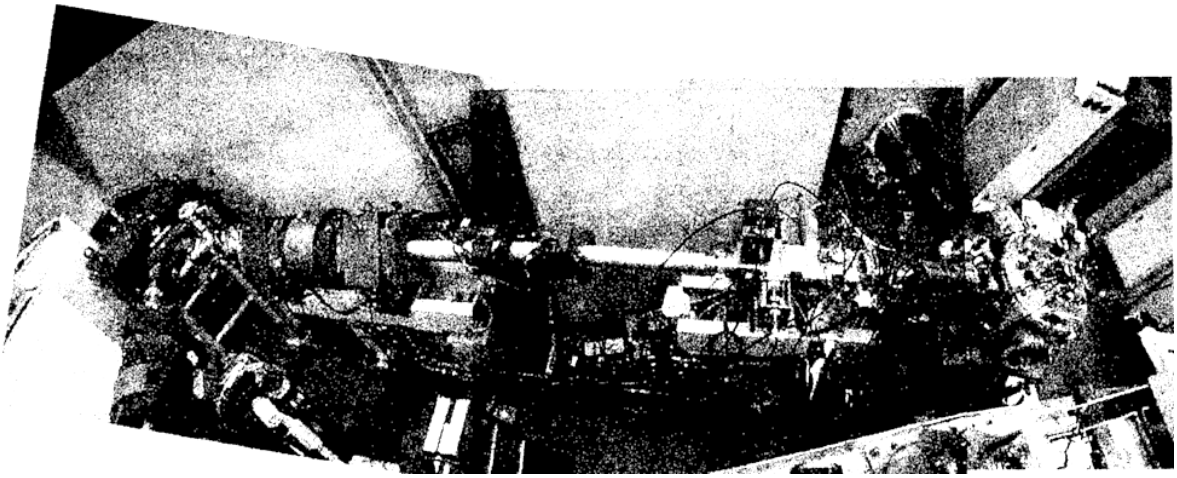

Fig. 1. Overview of Irradiation chamber of 42 beam course.

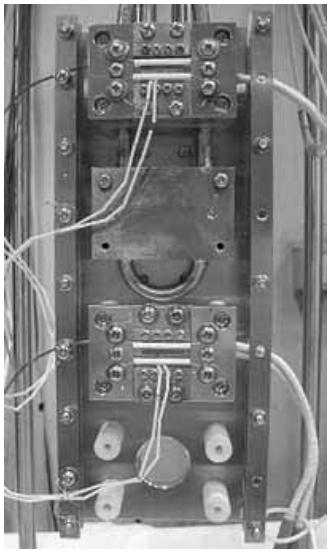

Fig. 2. Specimen loading system.

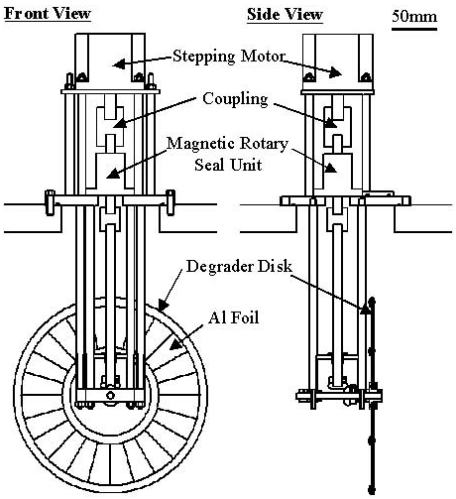

Fig. 3. Energy degrader.

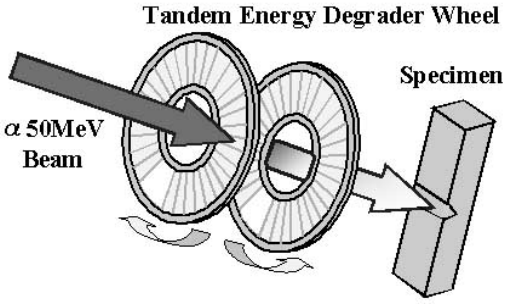

Fig. 4. Schematic view of a tandem degrader system.

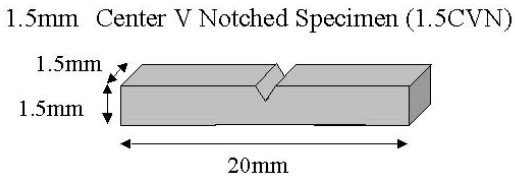

Fig. 5. Specimen size.

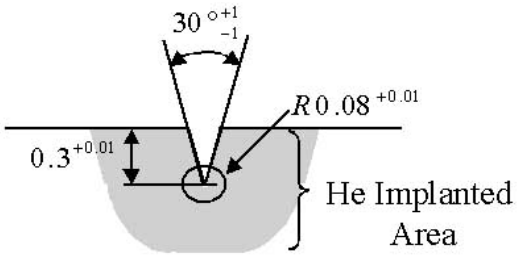

Fig. 6. Detail of V notch of the specimens.

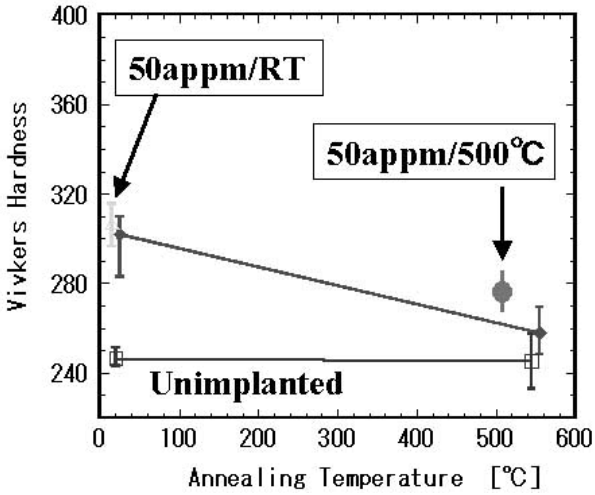

Fig. 7. Hardness of He implanted specimen.

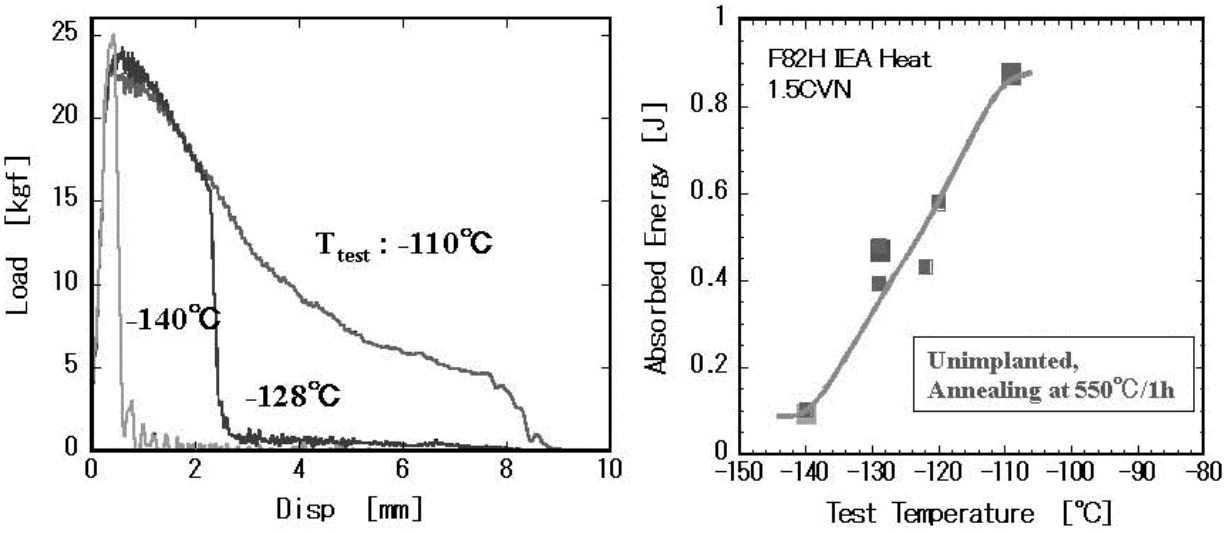

(a) (b)

Fig. 8. Load / Displacement curves by charpy test and absorbed energy / Test temperature curve of unimplanted sample.

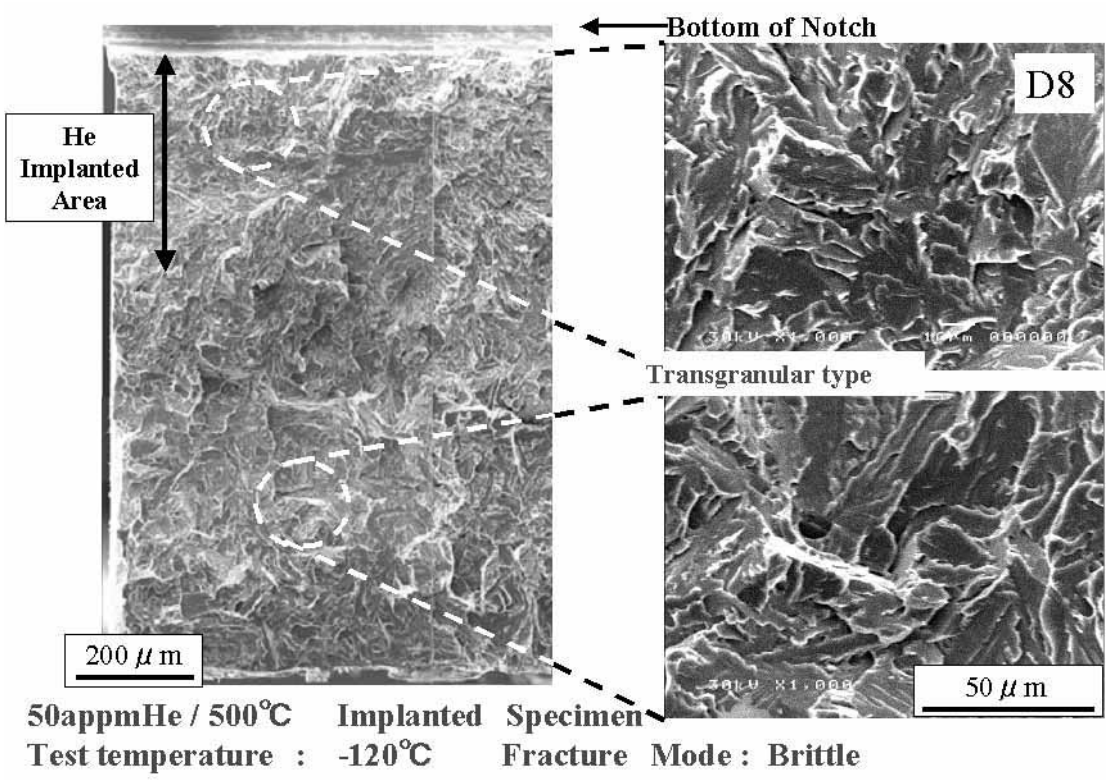

Fig. 9. Surface observation of ruptured 1.5CVN specimen in brittle mode.

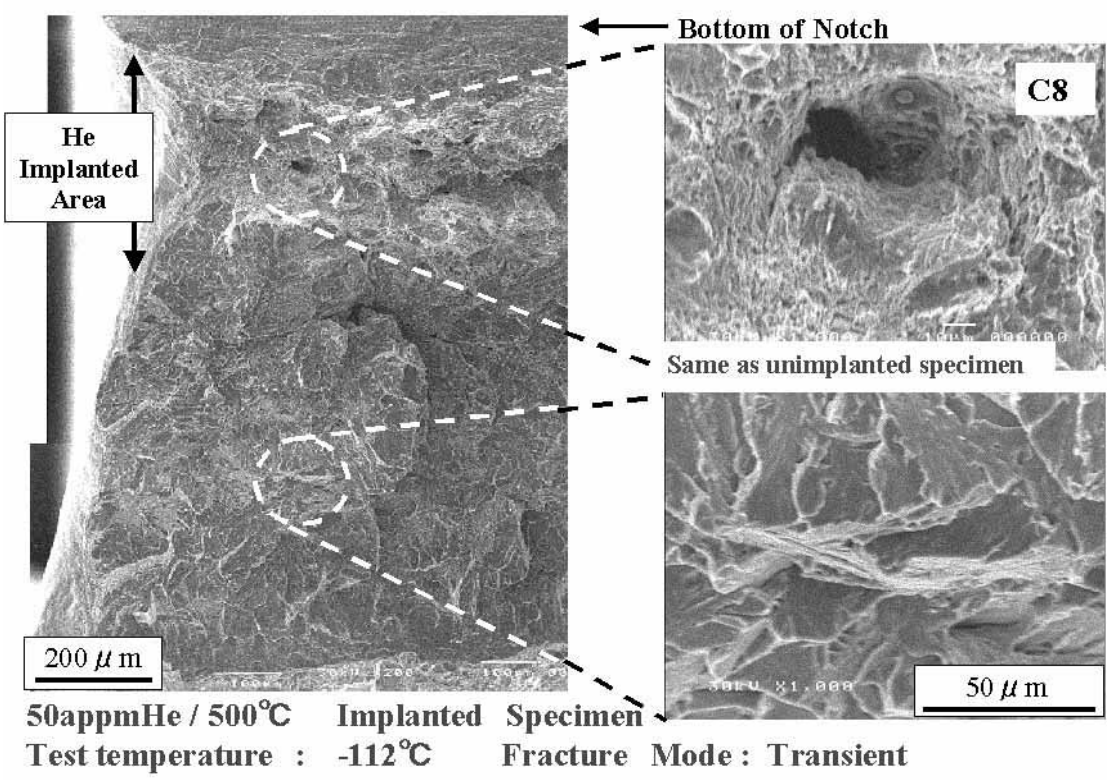

Fig. 10. Surface observation of ruptured 1.5CVN specimen in transient mode.

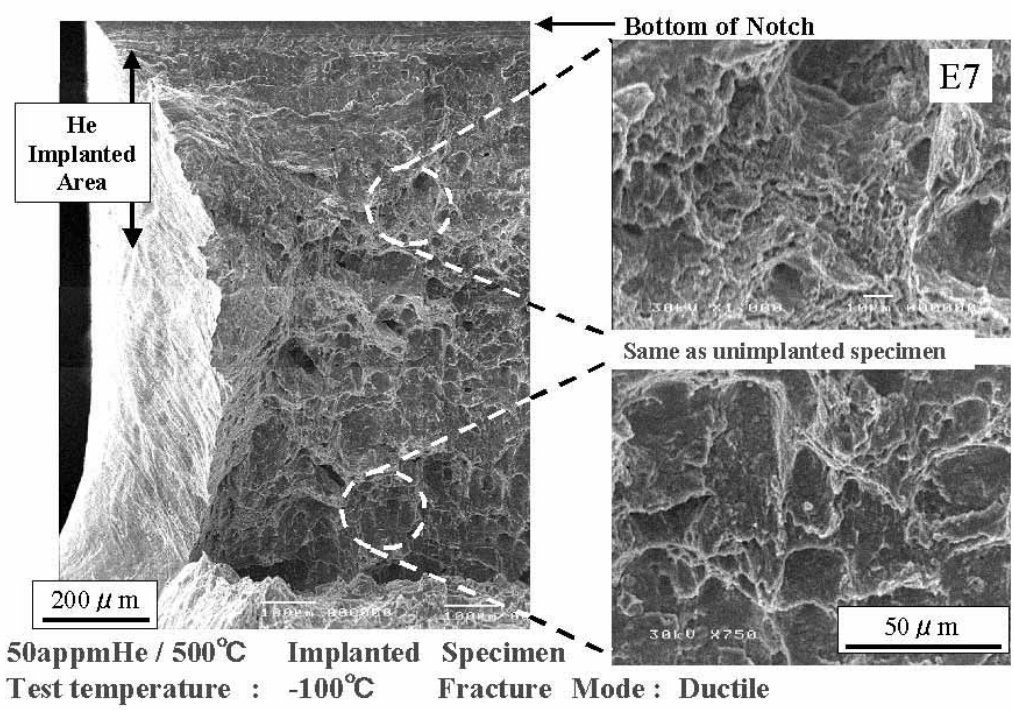

Fig. 11. Surface observation of ruptured 1.5CVN specimen in transient mode.

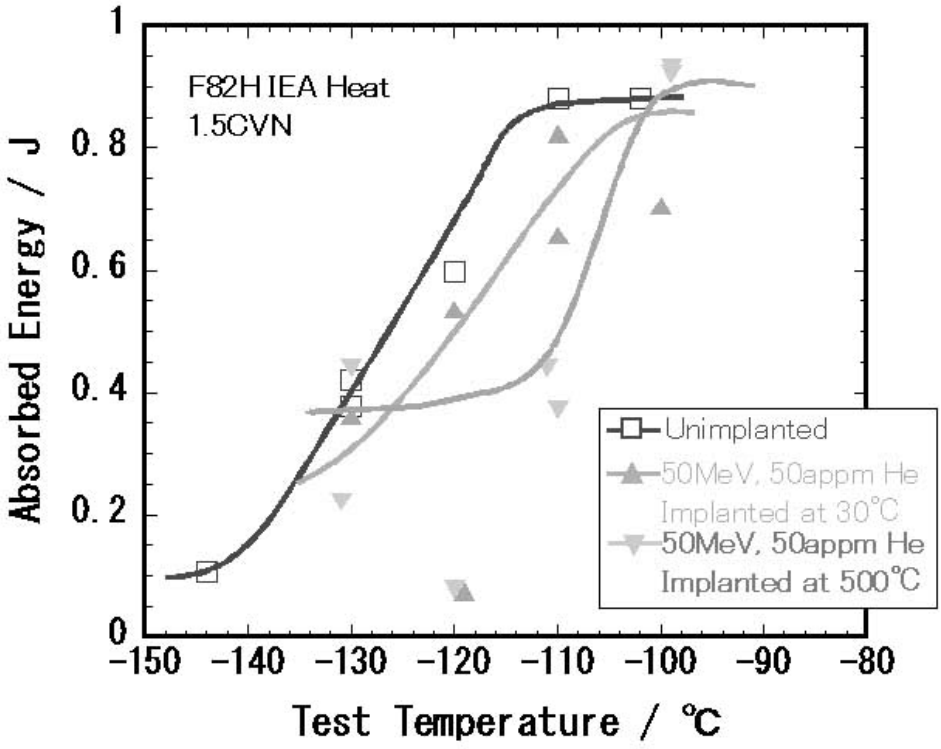

Fig. 12. Absorbed energy / Test temperature curves of He implanted samaple.